International Journal of Biological Macromolecules 129 (2019) 84–90

Contents lists available at ScienceDirect

International Journal of Biological Macromolecules

journal homepage: http://www.elsevier.com/locate/ijbiomac

A catechol biosensor based on immobilizing laccase to Fe_3O_4@Au core-shell nanoparticles

Changiz Karami *, Mohammad Ali Taher

Department of Chemistry, Faculty of Sciences, Shahid Bahonar University of Kerman, Kerman, Iran

ARTICLE INFO

Article history:
Received 25 November 2018
Received in revised form 6 January 2019
Accepted 3 February 2019
Available online 5 February 2019

Keywords:
Fe_3O_4@Au core-shell
Laccase immobilization
Biosensor
Catechol compound

ABSTRACT

This work is directed towards the synthesis of the magnetic nanoparticle in a core and a gold shell with immobilized of laccase on its surface (Fe_3O_4@Au@ Lac). The prepared Fe_3O_4@Au@ Lac core/shell nanoparticles are characterized by means TEM, SEM, DLS, zeta potential, UV-Vis, and TGA. Meanwhile, as an example of the applications, Biosensor activity was investigated by using the oxidation of catechol and recording the UV-Vis absorption in the 402 nm wavelength. The biosensor also demonstrated optimum activity at pH 5.0, reaction time at 40 min, and 35 mg the amount of biosensor. Linear response in the catechol concentration range of 5.0–70.0 μM. The limit of detection and the apparent Michaels–Menten constant (K_m) of the biosensor were 2 μM and 15 μM respectively.

1. Introduction

During the past few decades, The magnetic nanoparticles are very much considered because they are applied in various scientific fields such as purification of the protein, biological separation [1], target delivery [2], magnetic resonance imaging (MRI) [3], therapy [4], and biosensor [5,6]. One of the unique structures that the uniqueness of the structure due to the ability to functionalize in the surface as well as its magnetic properties is the Fe_3O_4 nanoparticle. In addition, it is easy to separate these compounds from the solution using the external magnetic field. Recently, much attention has been paid to the incorporation of magnetic materials with other functional components or other materials. Unique applicability with novel properties is the advantages of the new structures [7]. Among these compounds, the structure of the core-shell of iron-gold is much more attention due to the obvious benefits of Au nanoparticles. Gold is an inert element and very useful as a coating material for protecting magnetic nanoparticles, versatility in surface modification [8], high catalytic properties [9], and its unique biocompatibility [10].

In recent years, the environmental and toxicological problems are the addition of phenolic compounds, owing to the extensive use of these compounds in various industries, such as wood preservatives, textiles, surfactants, resins, herbicides, and pesticides [11–13]. One of the essential isomers of phenolic compounds is the catechol, which is widely used in various industries such as, antioxidants, pharmaceuticals, cosmetics, and so on. [14]. The sources of phenolic compounds are the natural decomposition of lingo-cellulosic and humic substances, all resulting in introducing catechol into nature. Because of the toxicity of this compound for humans, animals, and plants and also catechol easily absorbed by the digestive system. It causes a series of diseases like renal tube destruction, kidney pain and large doses induced strong suppression of the central nervous [15,16]. Due to the problems mentioned above, including the high toxicity and low degradability in the ecological environment, the detection of catechol has always been challenging for scientists and researchers.

Up to now, for identity, the catechol compounds several techniques have been used, including gas chromatography, capillary electrophoresis, and high-performance liquid chromatography, But these techniques are not cost-effective because of time-consuming and the instrumentations [17]. Compared to classical methods, the use of biosensors is a very remarkable alternative. The biosensor is simple to manufacture and operate, fast, highly selective, and appropriate for miniaturization and use as portable equipment [18,19].

One of these biosensor compounds is the laccase enzyme, the laccase (benzenediol: oxygen oxidoreductases, EC 1.10.3.2) enzyme is known as a multi-copper oxidase and is easily produced by numerous plants, fungus, and bacteria [20]. Compared to other enzymes that have oxidizing properties, Laccase is due to the high activity of a catalyst that the oxidation of a wide range of phenolic compounds, as well as low substrate specificity, which causes researchers to pay particular attention to the use of laccase as biosensors, a biofuel cell, and so on [21]. However, low stability and poor reusability of laccase have limited its further application [22]. As is known, one way to reduce the limitation of the use of the laccase with immobilization, thus increasing stability, durability and realizing continuous operations [23]. So far, various successful methods have been introduced with several types of carriers to immobilize the laccase including nanoparticles, membrane, nanofibers, and

* Corresponding author.
E-mail address: changiz.karami@gmail.com (C. Karami).

https://doi.org/10.1016/j.ijbiomac.2019.02.015
0141-8130/

microspheres [24–27]. Among these carriers, the magnetic nanoparticles are very simple and repeatable separated from the reaction medium in the presence of an external magnetic field. Therefore, this method reduces the operating costs in comparison with centrifugation and filtration [28]. However, to the best of our knowledge, No reports have been concerned with the immobilization of laccase on the core-shell nanoparticle of iron-gold, nor have any studies for the application of immobilized another enzyme on this nanoparticle. Even research on the use of this type of immobilized enzyme on the carrier has not been made.

Because of these problems, in this study, the magnetic nanoparticle is synthesized by the gold shell, and the laccase is immobilized on its surface. After characterization of this nano biosensor with various techniques such as TEM, SEM, DLS, zeta potential, UV-Vis, and TGA uses it as an optical biosensor to determine a catechol, which is one of the phenolic derivatives. Anyway, the aim of this study to synthesize a simple, easily prepared, inexpensive disposable biosensor for the determination of catechol in a water sample.

2. Experimental

2.1. Instrumental

For the study, the optical properties of the biosensor, a spectrophotometer (Cary 100) spectrometer was used. The hydrodynamic diameter of nanoparticle was characterized by dynamic light scattering (DLS, Malvern, ZEN3600). The diameter of the particles is measured using a transmission electron microscope (JEOL-JEM 2010). Using Thermo (AV-ATAR), in the wavenumber range 400–4000 cm^{-1} the FT-IR spectra have been recorded. The nanoparticle surface morphology has been investigated by FESEM (TESCAN, MIRA III). EDS and mapping by FESEM (TESCAN, MIRA III), The vibrating sample magnetometer (VSM, Lake Shore 7073) was used for characterization of magnetic properties of the nanoparticles.

2.2. Chemical and materials

Laccase from Trametes versicolor and PEI (branched, Mw = 1300 g/mol) were purchased from Sigma-Aldrich., EDC, NHS and MUA were obtained from Aldrich. Ferric chloride ($FeCl_3$ $6H_2O$, 99%), ferrous chloride ($FeCl_2$ $4H_2O$, 99%), Ammonium hydroxide, trisodium citrate dehydrate, N-Hydroxysuccinimide (NHS), 1-Ethyl-3-(3-dimethylaminopropyl) carbodiimide (EDC) and $HAuCl_4 \cdot 4H_2O$ (99.99%) were obtained from Merck. All chemicals materials are used with high purity and without further purification.

2.3. Immobilization of laccase

First, the magnetite nanoparticles (Fe_3O_4) [29] and then Fe_3O_4@Au@MUA as described in the supporting information, are synthesized so, for immobilize the laccase on the surface of the magnetic nanoparticle, carboxyl groups should be activated using NHS and EDC compounds. However, 20 mg of the modified nanoparticle)Fe_3O_4@Au@MUA(is mixed with 30 mM NHS and 150 mM EDC solution and stirred at room temperature for 3 h. After that, the Fe_3O_4@Au@MUA-NHS was incubated at 4 °C with 400 μL of 5 mg mL^{-1} of laccase solution (pH 6.8) for 24 h. In the end, using the magnets, remove the excess laccase from the reaction by washing with PBS (pH 6.8) and store the solution at 4 °C in the refrigerator [30].

2.4. Activity assays of free laccase

The Bradford method is used to calculate the amount of immobilized laccase on the surface of the magnetic nanoparticle. For this method, the protein concentration was measured using the Bradford method, and bovine albumin was used as a protein standard. This experiment was carried out at room temperature of ~25 °C [26].

2.5. Absorbance measurements

In 3 mL of deionized water amount 35 mg the corresponding Fe_3O_4@Au@Lac in phosphate buffer (pH 5.0) was added to a 1 cm path length quartz cell, then 0.1 mL × 5 μM of the corresponding catechol solution was added, we record changes in the absorbance at the working wavelengths at 402 nm with the use of the UV/Vis spectrum.

3. Results and discussion

The discussion of the results is divided into four sections. First, the synthesis of different steps of the magnetic biosensor is discussed, from the stage of synthesis of Fe_3O_4 to the stage of Fe_3O_4@Au@Lac. Second, the results of the magnetic biosensor (Fe_3O_4@Au@Lac) characterization are discussed. Third, the optimization of conditions such as reaction time, g of biosensor, pH, is discussed. And last, we discuss the laccase activities as well as kinetic parameters.

3.1. The synthesis of the magnetic bio-nanosensor

Scheme 1 illustrates the different stages of the synthesis of the Fe_3O_4@Au@Lac biosensor which are in four stages. First, the Fe_3O_4 nanoparticle is synthesized by a well-known method [31].then, reducing of the chloroauric acid with sodium citrate as a reducing agent to gold on the surface of a magnetic nanoparticle. Shell of gold on the surface of a

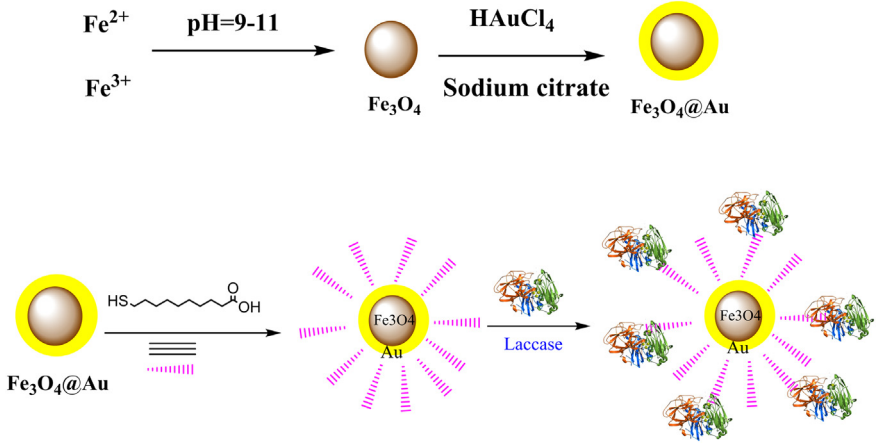

Scheme 1. Illustrates the different stages of the synthesis of the Fe_3O_4@Au@Lac.

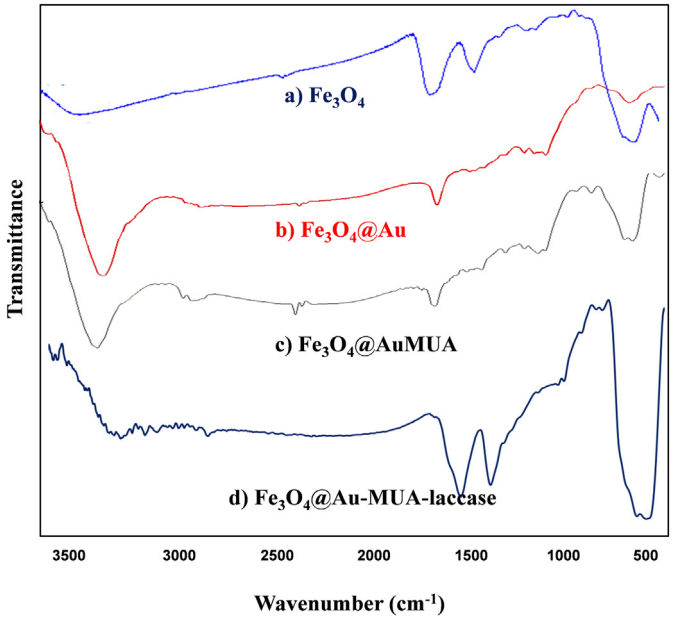

Fig. 1. The FTIR spectra of (a) the as-synthesized Fe_3O_4 nanoparticles, (b) Fe_3O_4@Au, (c) Fe_3O_4@Au-MUA, and (d) Fe_3O_4@Au-MUA conjugated with laccase.

magnetic nanoparticle has advantages, for example, it is an inert element that can protect the Fe_3O_4, and another important application is that it enables the structure to be used to create different functional groups on the surface. Third stages put the MUA on the surface of the core-shell of Fe_3O_4@Au nanomagnetic. MUA as a linker has a thiol and carboxylic acid group that hydroxyl groups create this freedom of action, which by activating them, materials that contain amine groups are easily placed on the surface of the nanomaterial. The final step in the synthesising of the biosensor is immobilized the enzyme on it, which is described in the experimental section, which first activates the carboxyl group, and then places the enzyme on the surface in a specific pH.

3.2. Characterization of Fe_3O_4@Au nanoparticles

For characterization of Fe_3O_4@Au@Lac the UV-Vis, FTIR, TEM, SEM, DLS, and VSM methods were used, as you know, the use of UV-Vis spectrophotometry is the most accessible method for characterization of core-shell of Fe_3O_4@Au. The observation of the surface plasmon resonance band in the UV-Vis spectrum shows indirect evidence of the formation of Fe_3O_4@Au core-shell morphology [32]. In Fig. 1S (Supplementary data), a different nanomagnetic structure such as Fe_3O_4 (a), Fe_3O_4@Au (b) and Fe_3O_4@Au-MUA (c) is compared. In contrast to the mostly silent feature in the visible region for Fe_3O_4 particles in Fig. 1S(a), whereas in Fig. 1S(b), in the area of 530 nm, there is an SP band due to the thick layer of Au on the surface of Fe_3O_4 particles. While similar SP band at 530 nm Au is clear in Fig. 1S(c) for Fe_3O_4@Au-MUA, but Due to the thin layer of MUA around Au, the SP band decreases slightly. The surface chemistry of the nanoparticles obtained in each step. Fig. 1 shows the FTIR spectra of (a) the as-synthesized Fe_3O_4 nanoparticles, (b) Fe_3O_4@Au, (c) Fe_3O_4@Au-MUA, and (d) Fe_3O_4@Au-MUA conjugated with laccase. The absorption bands at 630 and 440 cm^{-1}, characteristic of the Fe—O bond of Fe_3O_4, also the absorption bands at 1633.3 and 3432.5 cm^{-1} are assigned to bending and stretching vibrations of OH group respectively which results from the absorption of water molecules on the surface of Fe_3O_4 nanoparticles in all spectra imply the presence of the Fe_3O_4 nanoparticles in each step (Fig. 1(a)). In Fig. 1(b), Considering that capped nanoparticles with sodium citrate the FTIR peaks relate to citrate can be seen at 1610 cm^{-1} and 1380 cm^{-1} which is assigned to the asymmetry vibration of C═O. The peak around 3450 cm^{-1} related to stretching vibration of OH group and the peak around at 2966 cm^{-1} is associated with the stretching vibration of (CH_2) bond. Fig. 1(c) displays the FT-IR spectrum of the Fe_3O_4@Au-MUA, compared to Fe_3O_4@Au, there is a peak around 2900 cm^{-1} that is related to the symmetric and asymmetric stretching of the υa (CH_2). Therefore, the changes observed indicated that the surface of Fe_3O_4@Au was successfully modified with MUA. For the Fe_3O_4@Au-MUA bioconjugates (Fig. 1(d)), The main peaks that can be used to prove the binding of laccase to Fe_3O_4@Au-MUA are seen at 1570 and 1409 cm^{-1}, which are related to secondary amide C═O stretching as well as a peak in the 3290 cm^{-1}, which is related to hydroxyl groups of laccase. Therefore, FT-IR results provide evidential component information of different modified Fe_3O_4.

Fig. 2 was the SEM image of Fe_3O_4 and Fe_3O_4@Au-MUA bioconjugates; it can be concluded that the spherical shape particles have about 30 nm diameter. For comparison, the bare Fe_3O_4 was presented in Fig. 2(a) was relatively darker and more blurred than Fig. 2 (b) because the laccase coverage of Fe_3O_4 was much less electron dense than the substrate Fe_3O_4 [30].

The transmission electron microscope data provides significant evidence of core-shell formation (Fig. 3a,b). However, in the completion of SEM section, it is seen that the particle is spherical in shape with an

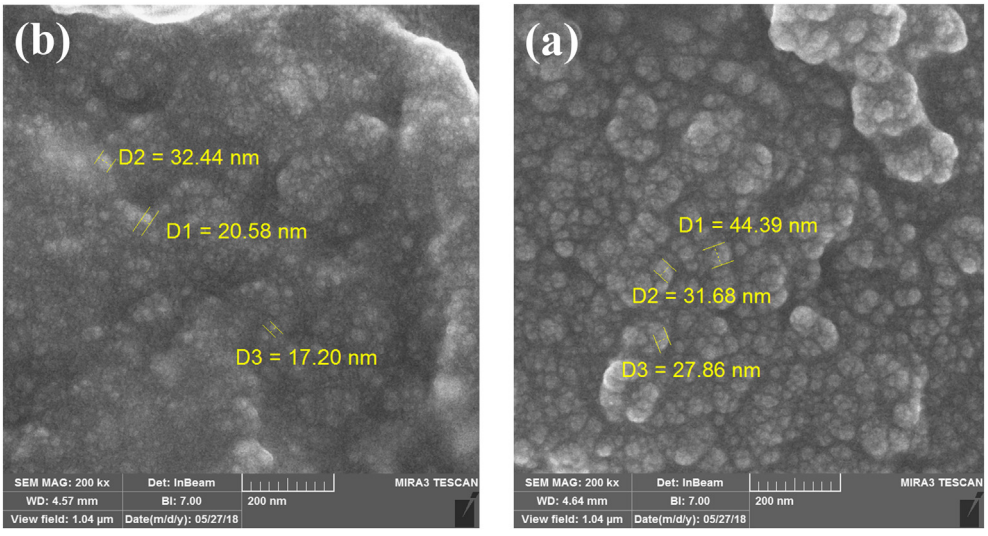

Fig. 2. SEM image of Fe_3O_4 and Fe_3O_4@Au-MUA bioconjugates.

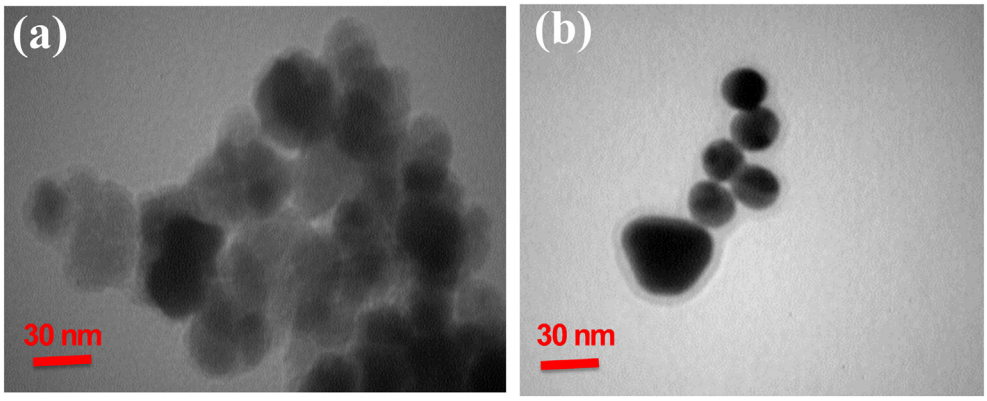

Fig. 3. TEM image of bare Fe_3O_4, and Fe_3O_4@Au core-shell.

average diameter of about 30 nm for both Fe_3O_4 states, bare and core-shell. Anyway, in Fig. 3(b), it is worth noting that the formation of a shell of Au with thickness average about 0.9 nm is evident.

The magnetic properties of the synthesized magnetic material are obtained using the vibrating sample magnetometer (VSM), in Fig. 4, the diagram of the Fe_3O_4 and Fe_3O_4@Au-MUA conjugated with laccase are shown. The saturation magnetization values of bare Fe_3O_4 and Fe_3O_4@Au-MUA conjugated with laccase were 63.7 and 50.98 emu/g, respectively. A significant decrease in the magnetic property of Fe_3O_4@Au-MUA conjugated with laccase in comparison of the Fe_3O_4 state is due to layers such as diamagnetic Au, MUA, and laccase in a surface of bare Fe_3O_4. By the way, due to decrease the magnetic strength, its strength is still enough to the separation of Fe_3O_4@Au-MUA conjugated with laccase from the solution for 3 mine using external magnet Fig. 4 (c). The Fe_3O_4 and Fe_3O_4@Au-MUA conjugated with laccase were measured through the TGA under nitrogen atmosphere condition at the heating rate of 15 °C/min, Fig. 2S(a, b) show the TGA curves. For Fig. 2S(a), which is related to as-prepared Fe_3O_4, the significant weight loss is from the 225–250 °C range, which is about 5%, due to the dehydroxylation of structural Fe-O [33]. In Fig. 6b, several times the weight loss in the curves is seen, the first stage is 80 °C, which is about 18% related to the adsorbed physical and chemical water. The second stage, beginning at 250 °C, which loses about 30% of its weight, is related to the dehydroxylation of structural Fe-O. While the other step up to 600 °C was due to the decomposition of other functional groups such as hydroxyl and carboxyl of laccase, thermogravimetric chart of Fe_3O_4@Au-MUA conjugated with laccase pointed that magnetite coated is about 60%. The energy dispersive X-ray spectra (EDS) result (Fig. 3S) confirms that the peaks of Au and S for gold shell and Cu for a layer of laccase were attributed to the Fe_3O_4@Au-MUA-laccase. These are evidence for the existence the layer of laccase and shell of gold in Fe_3O_4@Au. In addition, Fig. 4S which is related to the mapping, fully supports this information. The particle size and zeta potential of Fe_3O_4@Au-laccase are shown in Fig. 5S which the particle diameter is 470 nm and the zeta potential is −3.4 mV. As it is seen, a small but non-negligible difference between TEM and DLS data can be attributed to the following reasons. First of all, the diameter of the particle in the TEM is related to the metal core diameter, while the diameter of the particle in DLS is related to the sum of the core metal and the thickness of ligand layers, such as MUA and laccase. Second reason, the dynamic light scattering data is related to larger particles because the intensity of the scattering is proportional to the sixth power of particle size

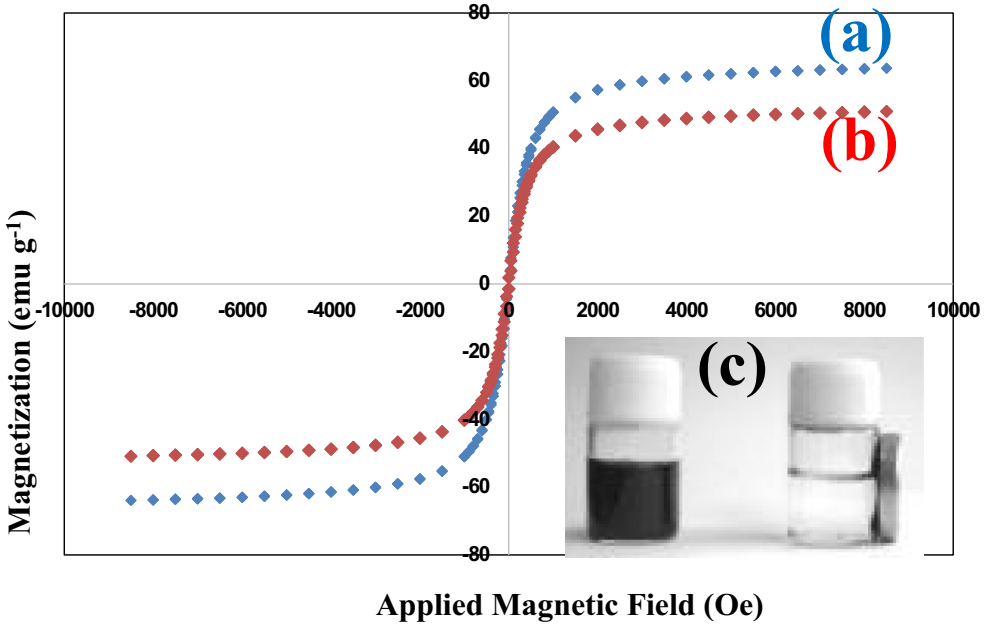

Fig. 4. Magnetization curves of (a) Fe3O4 and (b) Fe_3O_4@Au-MUA conjugated with laccase. (c) The photographs of Fe_3O_4@Au-MUA conjugated with laccase dispersed in solution (left) and separated from water solution under an external magnetic field (right).

[34]. Finally, the points that can be achieved from these interpretations are the particles uniformly distributed, and the surface of the Fe_3O_4 is modified with ligand layer and laccase.

3.3. Evaluation of biosensor response

The mechanism for detecting catechol by oxidation of it to quinone in the presence of an enzyme has been reported in previous researches, as shown in Fig. 6S [35]. Thereby, the oxidation makes it possible to monitor the amount of catechol by a new absorbance peak at a wavelength of 402 nm. Thus, the wavelength of 402 nm was used for monitoring the response of an optical biosensor. For better use of this biosensor, important parameters such as pH, time, and g of bio-sensor should be considered and the optimal conditions for this sensor are considered. The 35 mg of the biosensor was stirred in present of phosphate buffer solution (pH 5) and 5 μM of catechol for 40 min. The influence of pH on the biosensor response was investigated using phosphate buffer solutions at pH 3, pH 4, pH 5 to 6, and pH 7 (Fig. 6S). As seen in Fig. 6S, the optimal pH for biosensor was 5.0. While for pH values higher and lower than 5, the absorption rate is sharply decreased, which was probably due to a suppressed activity of laccase ($p < 0.05$) and damage incurred to enzyme structures in highly acidic conditions [36]. The effect of the biosensor amount (Fe_3O_4@Au-laccase) on the response is investigated by employing a various amount of the biosensor 7, 14, 35, and 40 mg. As shown in Fig. 7S, on increasing the biosensor amount to 35 mg the biosensor response increased which this increase in response is seen by increasing the absorption rate to reach a maximum value. The amount of laccase enzyme on the surface of the biosensor is calculated using the Bradford method that is described in the experimental section, so, for a 1 mg of a biosensor, 0.07 mg of the laccase enzyme was loaded. The time is the last parameter that is considered for optimized conditions for evaluation of biosensor response. To 35 mg of biosensor added 5 μM of catechol in pH 5 and record absorption at different times from 10 to 60 min, which can be seen the 40 min to be the best time.

3.4. Activity assays

The biosensor activity assay was performed by the amount of catechol oxidation in optimize conditions with different concentrations of substrate. In Fig. 5a, the Michaelis–Menten curve (V_0 versus substrate concentration [S]) shows the relationship between the enzymes (at constant concentration) or a structure that has an enzyme and the concentration of the substrate. V_0 is the initial rate of production of the enzyme product. In the Michaelis–Menten curve, with an increase in the value of [S], the amount of V_0 increases up to where this increase is eventually independent of [S], and the velocity at which this occurs is called V_{max}, and it is the fastest that the given amount of enzyme can operate.

Table 1
Comparing kinetic parameters of some laccases.

Enzyme	K_m (μM)	V_m μM/min	References
Laccase from Trametes versicolor	95.5	755	Nazari et al. [17]
Laccase from Ganoderma lucidum	521	19.6	Xu et al. [36]
Laccase from Botrytis cinerea	100	–	Sun et al. [38]
Laccase from Mycena purpureofusca	296	64.5	You et al. [37]
Laccase from immobilizing to Fe_3O_4@Au core-shell	15	4.3	Present work

Another parameter that is important in the Michaelis–Menten curve is K_m constant. K_m is important since it indicates the [S] at which the enzyme is most effective at altering the rate of the reaction. Therefore, for the study of enzyme activities, the characterization of K_m and V_{max} are two important parameters and significant. To determining the value of V_{max} and K_m, the Lineweaver–Burk plot (1) is used which is V_0 at different concentrations of [S]. The V_{max} and K_m were calculated from the Lineweaver–Burk plot to be 4.3 nM/min and 15 μM, respectively (Fig. 5b). In Table 1, the kinetic constants V_{max} and K_m of the kinetic parameters of laccase of this research has been investigated and compared with the previous work, which shows that K_m values are much less than the other laccases which indicate that this enzyme has higher substrate affinity [17,37–39].

$$1/V_0 = K_m/V_{max} \times 1/[S] + 1/V_{max} \quad (1)$$

3.5. The sensitivity

Fig. 6a shows the response curve of the biosensor towards catechol in the range of 0.0–80 μM. As shown, a linear response of the biosensor was observed in the catechol concentration range of 5–70 μM. Moreover, the increase of catechol concentration induced the increase of the absorption at a 402 nm band with a linear relationship ($y = 0.0026x + 0.1022$) and the sensitivity by R is 98% (Fig. 6b). As such, Fe_3O_4@Au-laccase as a biosensor can be used for the colourimetric detection of catechol and the calculated limit of detection (LOD) was about 2 μM according to the $S/N = 3$ rule. By comparing the linear range and detection limit with other researches, the performance of sensing of catechol was compared with laccase and tyrosinase immobilized in different matrices. In Table.2, clearly shows the appropriate linear range and also the detection limit better or lower in comparison to some of the other researches [16,35,40–43].

4. Conclusion

In this research, the novel and easy route for detection of catechol by a Uv/vis spectrophotometer were introduced. Using the reduction of gold salt in the presence of citrate as a reducing agent for preparation of the core-shell of Fe_3O_4@Au, and the surface of the gold-coated

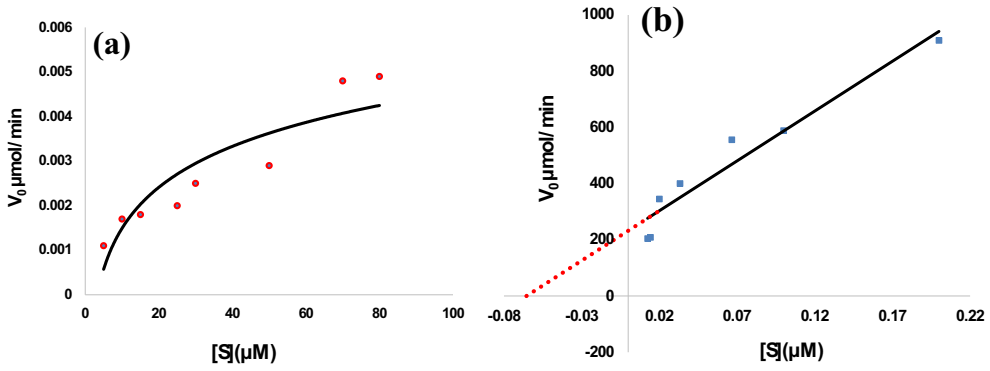

Fig. 5. (a) The Michaelis–Menten curve. (b) Lineweaver–Burk plot.

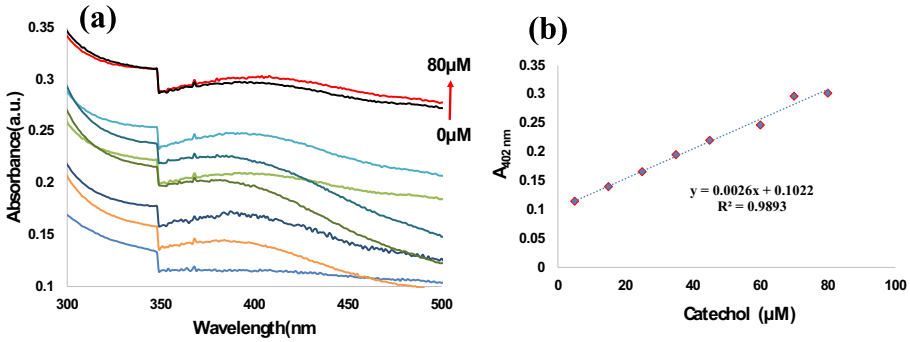

Fig. 6. (a) the response curve of the biosensor towards catechol in the range of 0.0–80 μM, pH 5.0, (b) increase in the relative sensitivity of the detection system with respect to the concentration of the catechol.

Table 2
Comparing sensing of catechol with laccase and tyrosinase immobilized in different matrices.

Biosensor	Linear range	Detection limit	References
Tyrosinase extract immobilized into a sol–gel silica layered matrix	50–400 μM	52 μM	Leboukh et al. [16]
Immobilization of tyrosinase in chitosan	2.5–100.0 μM	1.0 μM	Berne and Pecora [34]
Tyrosinase immobilization on functionalized porous silicon surface	1–100 μM	0.43 μM	Slomczynski et al. [39]
polymer hydrogel microparticles and enzyme–quantum dot conjugates	200–800 μM	–	Lasmi et al. [40]
Immobilization of Laccase and MBTH in Stacked Films	0.5–8.0 mM	0.33 mM	Park et al. [41]
Hybrid nafion/sol–gel silicate for MBTH immobilization	0.5–10.0 mg/L	0.23 mg/L	Abdullah et al. [42]
immobilizing laccase to Fe3O4@Au core-shell nanoparticles	5.0–70.0 μM	2 μM	Present work

magnetic nanoparticle modified by MUA. Then, to immobilize the laccase on the surface of the magnetic nanoparticle, carboxyl groups should be activated using NHS and EDC compounds. The obtained particles were characterized by TEM, SEM, DLS, zeta potential, UV-Vis, and TGA. The results revealed, the linear range, sensitivity by R, and detection limit for this biosensor were obtained 5–70 μM, 98%, 2 μM respectively. The developed biosensor has a good potential use in quantitative determination of catechol compound in water solution.

Acknowledgement

We are thankful to the Department of Chemistry, Faculty of Sciences, Shahid Bahonar University of Kerman, Kerman, Iran for the support of this work.

Appendix A. Supplementary data

Supplementary data to this article can be found online at https://doi.org/10.1016/j.ijbiomac.2019.02.015.

References

[1] T.T.H. Pham, C. Cao, S.J. Sim, Application of citrate-stabilized gold-coated ferric oxide composite nanoparticles for biological separations, J. Magn. Magn. Mater. 320 (15) (2008) 2049–2055.
[2] S. Guo, D. Li, L. Zhang, J. Li, E. Wang, Monodisperse mesoporous superparamagnetic single-crystal magnetite nanoparticles for drug delivery, Biomaterials 30 (10) (2009) 1881–1889.
[3] K.L. Hultman, A.J. Raffo, A.L. Grzenda, P.E. Harris, T.R. Brown, S. O'Brien, Magnetic resonance imaging of major histocompatibility class II expression in the renal medulla using immunotargeted superparamagnetic iron oxide nanoparticles, ACS Nano 2 (3) (2008) 477–484.
[4] J. Kim, S. Park, J.E. Lee, S.M. Jin, J.H. Lee, I.S. Lee, I. Yang, J.S. Kim, S.K. Kim, M.H. Cho, Designed fabrication of multifunctional magnetic gold nanoshells and their application to magnetic resonance imaging and photothermal therapy, Angew. Chem. 118 (46) (2006) 7918–7922.
[5] T. Zhang, W. Wang, D. Zhang, X. Zhang, Y. Ma, Y. Zhou, L. Qi, Biotemplated synthesis of gold nanoparticle–bacteria cellulose nanofiber nanocomposites and their application in biosensing, Adv. Funct. Mater. 20 (7) (2010) 1152–1160.
[6] T.T. Baby, S. Ramaprabhu, SiO_2 coated Fe_3O_4 magnetic nanoparticle dispersed multiwalled carbon nanotubes based amperometric glucose biosensor, Talanta 80 (5) (2010) 2016–2022.
[7] P. Lu, J.-L. Zhang, Y.-L. Liu, D.-H. Sun, G.-X. Liu, G.-Y. Hong, J.-Z. Ni, Synthesis and characteristic of the Fe3O4@ SiO2@ Eu (DBM) $3{\cdot}2H_2O/SiO_2$ luminomagnetic microspheres with core-shell structure, Talanta 82 (2) (2010) 450–457.
[8] X. Zhao, Y. Cai, T. Wang, Y. Shi, G. Jiang, Preparation of alkanethiolate-functionalized core/shell Fe3O4@ Au nanoparticles and its interaction with several typical target molecules, Anal. Chem. 80 (23) (2008) 9091–9096.
[9] S. Goergen, C. Yin, M. Yang, B. Lee, S. Lee, C. Wang, P. Wu, M. Boucher, G. Kwon, S. Seifert, Structure sensitivity of oxidative dehydrogenation of cyclohexane over FeOx and Au/Fe_3O_4 nanocrystals, ACS Catal. 3 (4) (2013) 529–539.
[10] K.C. Grabar, R.G. Freeman, M.B. Hommer, M.J. Natan, Preparation and characterization of Au colloid monolayers, Anal. Chem. 67 (4) (1995) 735–743.
[11] C. Xu, J. Wang, J. Zhou, Nanoporous PtNi alloy as an electrochemical sensor for ethanol and H2O2, Sensors Actuators B Chem. 182 (2013) 408–415.
[12] R.S. Freire, M.M. Ferreira, N. Durán, L.T. Kubota, Dual amperometric biosensor device for analysis of binary mixtures of phenols by multivariate calibration using partial least squares, Anal. Chim. Acta 485 (2) (2003) 263–269.
[13] M.A. McKinney, L.S. Cesh, J.E. Elliott, T.D. Williams, D.K. Garcelon, R.J. Letcher, Brominated flame retardants and halogenated phenolic compounds in North American west coast bald eaglet (Haliaeetus leucocephalus) plasma, Environ. Sci. Technol. 40 (20) (2006) 6275–6281.
[14] R. Subramanyam, I. Mishra, Biodegradation of catechol (2-hydroxy phenol) bearing wastewater in an UASB reactor, Chemosphere 69 (5) (2007) 816–824.
[15] R.S. Freire, N. Durán, L.T. Kubota, Electrochemical biosensor-based devices for continuous phenols monitoring in environmental matrices, J. Braz. Chem. Soc. 13 (4) (2002) 456–462.
[16] S. Leboukh, H. Gouzi, T. Coradin, H. Yahia, An optical catechol biosensor based on a desert truffle tyrosinase extract immobilized into a sol–gel silica layered matrix, J. Sol-Gel Sci. Technol. (2018) 1–7.
[17] M. Nazari, S. Kashanian, R. Rafipour, Laccase immobilization on the electrode surface to design a biosensor for the detection of phenolic compound such as catechol, Spectrochim. Acta A Mol. Biomol. Spectrosc. 145 (2015) 130–138.
[18] T.-T. Xia, C.-Z. Liu, J.-H. Hu, C. Guo, Improved performance of immobilized laccase on amine-functioned magnetic Fe3O4 nanoparticles modified with polyethylenimine, Chem. Eng. J. 295 (2016) 201–206.
[19] D.-M. Liu, J. Chen, Y.-P. Shi, Tyrosinase immobilization on aminated magnetic nanoparticles by physical adsorption combined with covalent crosslinking with improved catalytic activity, reusability and storage stability, Anal. Chim. Acta 1006 (2018) 90–98.
[20] M. Fernández-Fernández, M.Á. Sanromán, D. Moldes, Recent developments and applications of immobilized laccase, Biotechnol. Adv. 31 (8) (2013) 1808–1825.
[21] P. Giardina, V. Faraco, C. Pezzella, A. Piscitelli, S. Vanhulle, G. Sannia, Laccases: a never-ending story, Cell. Mol. Life Sci. 67 (3) (2010) 369–385.
[22] H. Cabana, A. Ahamed, R. Leduc, Conjugation of laccase from the white rot fungus Trametes versicolor to chitosan and its utilization for the elimination of triclosan, Bioresour. Technol. 102 (2) (2011) 1656–1662.

[23] A. Kunamneni, I. Ghazi, S. Camarero, A. Ballesteros, F.J. Plou, M. Alcalde, Decolorization of synthetic dyes by laccase immobilized on epoxy-activated carriers, Process Biochem. 43 (2) (2008) 169–178.
[24] A. Babadostu, O.K. Guldu, D.O. Demirkol, E.I. Medine, P. Unak, S. Timur, Affinity based laccase immobilization on modified magnetic nanoparticles: biosensing platform for the monitoring of phenolic compounds, Int. J. Polym. Mater. Polym. Biomater. 64 (5) (2015) 260–266.
[25] R. Xu, Y. Si, X. Wu, F. Li, B. Zhang, Triclosan removal by laccase immobilized on mesoporous nanofibers: strong adsorption and efficient degradation, Chem. Eng. J. 255 (2014) 63–70.
[26] B. Karagoz, G. Bayramoglu, B. Altintas, N. Bicak, M.Y. Arica, Amine functional monodisperse microbeads via precipitation polymerization of N-vinyl formamide: immobilized laccase for benzidine based dyes degradation, Bioresour. Technol. 102 (13) (2011) 6783–6790.
[27] J. Hou, G. Dong, Y. Ye, V. Chen, Enzymatic degradation of bisphenol-A with immobilized laccase on TiO_2 sol–gel coated PVDF membrane, J. Membr. Sci. 469 (2014) 19–30.
[28] A. Pich, S. Bhattacharya, H.J.P. Adler, T. Wage, A. Taubenberger, Z. Li, K.H. van Pee, U. Böhmer, T. Bley, Composite magnetic particles as carriers for laccase from Trametes versicolor, Macromol. Biosci. 6 (4) (2006) 301–310.
[29] W. Yantasee, Y. Lin, G.E. Fryxell, B.J. Busche, J.C. Birnbaum, Removal of heavy metals from aqueous solution using novel nanoengineered sorbents: self-assembled carbamoylphosphonic acids on mesoporous silica, Sep. Sci. Technol. 38 (15) (2003) 3809–3825.
[30] H. Qiu, C. Xu, X. Huang, Y. Ding, Y. Qu, P. Gao, Immobilization of laccase on nanoporous gold: comparative studies on the immobilization strategies and the particle size effects, J. Phys. Chem. Lett. 113 (6) (2009) 2521–2525.
[31] S. Karamipour, M. Sadjadi, N. Farhadyar, Fabrication and spectroscopic studies of folic acid-conjugated Fe_3O_4@Au core–shell for targeted drug delivery application, Spectrochim. Acta A Mol. Biomol. Spectrosc. 148 (2015) 146–155.
[32] L. Wang, L. Wang, J. Luo, Q. Fan, M. Suzuki, I.S. Suzuki, M.H. Engelhard, Y. Lin, N. Kim, J.Q. Wang, Monodispersed core−shell Fe_3O_4@Au nanoparticles, J. Phys. Chem. B 109 (46) (2005) 21593–21601.
[33] J. Xie, C. Xu, N. Kohler, Y. Hou, S. Sun, Controlled PEGylation of monodisperse Fe_3O_4 nanoparticles for reduced non-specific uptake by macrophage cells, Adv. Mater. 19 (20) (2007) 3163–3166.
[34] B. Berne, R. Pecora, Dynamic Light Scattering with Applications to Chemistry, Biology and Physics, Wiley, New York, 1976.
[35] J. Abdullah, M. Ahmad, N. Karuppiah, L.Y. Heng, H. Sidek, Immobilization of tyrosinase in chitosan film for an optical detection of phenol, Sensors Actuators B Chem. 114 (2) (2006) 604–609.
[36] R. Xu, Q. Zhou, F. Li, B. Zhang, Laccase immobilization on chitosan/poly (vinyl alcohol) composite nanofibrous membranes for 2,4-dichlorophenol removal, Chem. Eng. J. 222 (2013) 321–329.
[37] L.F. You, Z.M. Liu, J.F. Lin, L.Q. Guo, X.L. Huang, H.X. Yang, Molecular cloning of a laccase gene from Ganoderma lucidum and heterologous expression in Pichia pastoris, J. Basic Microbiol. 54 (S1) (2014) S134–S141.
[38] S. Sun, Y. Zhang, Y. Que, B. Liu, K. Hu, L. Xu, Purification and characterization of fungal laccase from Mycena purpureofusca, Chiang Mai J. Sci. 40 (2013) 151–160.
[39] D. Slomczynski, J. Nakas, S. Tanenbaum, Production and characterization of laccase from Botrytis cinerea 61-34, Appl. Environ. Microbiol. 61 (3) (1995) 907–912.
[40] K. Lasmi, H. Derder, A. Kermad, S. Sam, H. Boukhalfa-Abib, S. Belhousse, F.Z. Tighilt, K. Hamdani, N. Gabouze, Tyrosinase immobilization on functionalized porous silicon surface for optical monitoring of pyrocatechol, Appl. Surf. Sci. 446 (2018) 3–9.
[41] S.-A. Park, E. Jang, W.-G. Koh, B. Kim, Fabrication and characterization of optical biosensors using polymer hydrogel microparticles and enzyme–quantum dot conjugates, Sensors Actuators B Chem. 150 (1) (2010) 120–125.
[42] J. Abdullah, M. Ahmad, L.Y. Heng, N. Karuppiah, H. Sidek, An optical biosensor based on immobilization of laccase and MBTH in stacked films for the detection of catechol, Sensors 7 (10) (2007) 2238–2250.
[43] J. Abdullah, M. Ahmad, L.Y. Heng, N. Karuppiah, H. Sidek, Chitosan-based tyrosinase optical phenol biosensor employing hybrid nafion/sol–gel silicate for MBTH immobilization, Talanta 70 (3) (2006) 527–532.